Ab initio calculations of the main crystal surfaces of forsterite (M2SiO4): a preliminary study to understand the nature of geochemical processes at the olivine interface

(Article begins on next page)

21 June 2024

Ab Initio Calculations of the Main Crystal Surfaces of Forsterite (Mg$_2$SiO$_4$): A Preliminary Study to Understand the Nature of Geochemical Processes at the Olivine Interface

BRUNO M.,*[1] MASSARO F. R.,[2] PRENCIPE M.,[1] DEMICHELIS R.,[3] DE LA PIERRE M.,[4] NESTOLA F.[2]

[1] Dipartimento di Scienze della Terra, Università degli Studi di Torino, Via Valperga Caluso 35, 10125 Torino, Italy.

[2] Dipartimento di Geoscienze, Università degli Studi di Padova, Via Gradenigo 6, 35131 Padova, Italy.

[3] Nanochemistry Research Institute, Department of Chemistry, Curtin University, PO Box U1987, Perth, WA 6845, Australia.

[4] Dipartimento di Chimica, Università degli Studi di Torino and NIS -Nanostructured Interfaces and Surfaces - Centre of Excellence, Via P. Giuria 7, 10125 Torino, Italy.

ABSTRACT: We present an accurate *ab initio* study of the structure and surface energy at 0 K of the (010), (101), (111), (001), (110), (120) and (021) faces of forsterite (Mg$_2$SiO$_4$), by using the hybrid Hartree-Fock/Density Functional B3LYP Hamiltonian and a localized all-electron Gaussian-type basis set. According to the surface energy values, the stability order of the forsterite faces results to be (010) < (120) < (001) < (101) < (111) < (021) < (110). Then, the equilibrium shape of forsterite is drawn and compared with the previous ones obtained at empirical level.

Our results are combined with experimental evidences to develop some considerations about the shape and genesis of olivine included in diamond. They provide crucial information on the diamond formation mechanism with respect to its guest inclusions, a topic which is still under strong debate in the scientific community. In particular, we have discussed the peculiar crystal morphology of olivine included in diamond and we have demonstrated that it cannot be considered as an evidence of syngenesis (i.e., inclusion and host diamond formed at the same time). Furthermore, if the morphology of olivine was modified during its encapsulation in diamond, but it does not show a preferential orientation with respect to diamond, we can state that: (i) the *bulk* of olivine is protogenetic (i.e., a piece of previously formed olivine is encapsulated by the host diamond), whereas (ii) its *shape* is syngenetic, that is the morphology is rearranged during the encapsulation.

1. Introduction

Olivine exists as a complete isomorphous series, with composition ranging from forsterite (Mg_2SiO_4) to fayalite (Fe_2SiO_4), but the most common olivines are richer in magnesium than in iron.[1] Other than being one of the major components of the Earth's mantle and of many meteorite classes, it is often detected on the surface of extra-terrestrial planetary bodies and, more generally, in the spectra of astronomical targets.[2] As a consequence, olivine plays a fundamental role in defining the properties, in influencing the physico-chemical processes and in recording the history of both terrestrial and extra-terrestrial environments.[3-6]

Within the wide family of natural phenomena that involve olivine, of particular interest are those occurring at the interface between olivine and other materials, such as minerals and water environments. For example, the olivine/water interface is increasingly raising the attention of the whole international scientific community due the natural and widespread occurrence of reactions that can lead to i) carbon dioxide storage; ii) the production of hydrogen and the synthesis of organic molecules; iii) the formation of serpentines (lizardite, antigorite, chrysotile).[7-10]

An important process where the olivine/mineral interface plays a fundamental role is relative to the inclusions of olivine in diamond (DIs). Such inclusions, together with other silicates, oxide and sulfides found in diamonds are among the deepest materials originating from Earth's interior and reaching the planet surface. Diamonds are billion years old and remain unaltered over time preserving the pristine conditions of Earth. Therefore, their study plays a key role in understanding and interpreting the geodynamics, geophysics, petrology, geochemistry and mineralogy of Earth's mantle from the lithospheric to the lowermost part (see Stachel and Harris,[11] and references therein).

A comprehensive knowledge of olivine surface energetics and morphology at the atomic level is of extreme importance to understand the true nature of these and, more generally, all those processes involving the olivine interface. However, to the authors' knowledge, there are only a few studies that address this issue, and they all deal with the Mg end member only (forsterite). In particular, two computational studies based on force field calculations have been performed on the main surfaces of forsterite,[12,13] whereas all of the other computational studies in the literature deal with the adsorption of H, H_2 and H_2O on the (010) surface.[14-19]

In this paper we present a preliminary study to provide a new insight into the structure and energetics of the crystal faces of forsterite, by means of *ab initio* quantum-mechanics calculations and a two-dimensional slab model. In particular, the equilibrium geometry and the surface energy at 0 K of the (010), (101), (111), (001), (110), (120) and (021) faces of forsterite were determined. These results were then combined with experimental evidences to develop some considerations

about the shape and genesis of olivine included in diamond, which displays, as we will show in the following, a very different crystal morphology with respect to that of olivine crystals not entrapped inside the diamond and to the equilibrium shape determined in this work. We proposed an explanation accounting for these differences, by demonstrating that our results could provide crucial information on the diamond formation mechanism with respect to its guest inclusions, a topic that is still under strong debate in the scientific community.

Furthermore, as future computational works of our research group will be devoted to the study of the structure and energy of diamond/olivine interfaces (in order to study the epitaxial relationships between these phases and to estimate the shape of olivine crystals included in diamond), the first step for such investigation is the assessment of our quantum mechanical *ab initio* method in the description of clean olivine surfaces. Therefore, the present paper can also be considered an essential work to set the best computational parameters to use in the ab initio calculations that will be performed for simulating the diamond/olivine interfaces.

A hybrid Hartree-Fock (HF)-DFT approach was adopted, which notably has never been applied before to the study of olivine surfaces. In particular, the B3LYP[20-22] functional was used, which has already demonstrated great accuracy in describing the surfaces of diamond,[23] as well as the structural, vibrational and thermophysical properties of forsterite and fayalite.[24-28]

The paper is structured as follows: (i) outline of the adopted computational methodology; (ii) description of the structure and energy of the surfaces, and comparison with previous computational studies; (iii) application of computational findings to understand the shape and genesis of olivine included in diamonds, and (iv) main conclusions.

2. Computational details

The calculations were performed at the DFT (Density Functional Theory) level with the periodic *ab initio* CRYSTAL09 code.[29-31] The hybrid B3LYP[20-22] Hamiltonian, already shown to provide accurate results for structural and dynamical properties of olivine end members,[24-26,28] was employed. Crystal surfaces were simulated by using a 2D periodic slab model, consisting of a film formed by a set of atomic layers parallel to the *hkl* crystalline plane of interest.[32] The output files are freely available at http://mabruno.weebly/download.

In CRYSTAL the multi-electronic wave-function is constructed as an anti-symmetrized product (Slater determinant) of mono-electronic crystalline orbitals (COs) which are linear combinations of local functions (i.e. atomic orbitals, AOs) centered on each atom of the crystal. In turn, AOs are linear combinations of Gaussian-type functions (GTF, the product of a Gaussian times a real solid spherical harmonic to give *s*-, *p*- and *d*-type AOs). In this study, silicon, oxygen,

and magnesium were described by (8s)−(6311sp)−(1d), (8s)−(411sp)−(1d), and (8s)−(511sp)−(1d) contractions, respectively. The exponents (in bohr^{-2} units) of the most diffuse sp shells are 0.32 and 0.13 (Si), 0.59 and 0.25 (O), and 0.68 and 0.22 (Mg); the exponents of the single Gaussian d shell are 0.6 (Si), 0.5 (O), and 0.5 (Mg).[26,28]

The thresholds controlling the accuracy in the evaluation of Coulomb and exchange integrals (ITOL1, ITOL2, ITOL3, ITOL4 and ITOL5, see Dovesi et al.[29]) were set to 10^{-8} (ITOL1 to ITOL4) and 10^{-16} (ITOL5). The threshold on the SCF energy was set to 10^{-8} Hartree.

In the adopted package the DFT exchange and correlation contributions are evaluated by numerically integrating functions of the electron density and of its gradient over the cell volume. The choice of the integration grid is based on an atomic partition method, originally developed by Becke.[33] In the present study, a *pruned* (75, 974) p grid was adopted (XLGRID in the code[29]), which ensured a satisfactory accuracy in the numerically integrated electron charge density (the error is on the order of 1·10^{-4} |e| on a total of 1120 |e| for all the considered surfaces).

The reciprocal space was sampled according to a Monkhorst-Pack mesh[34] with shrinking factor 4, corresponding to 10 **k** points in the first irreducible Brillouin zone.

Structures were optimized by using the analytical energy gradients with respect to atomic coordinates and lattice parameters within a quasi-Newton scheme, combined with the Broyden-Fletcher-Goldfarb-Shanno scheme for Hessian updating.[35-37] Convergence was checked on energy, gradient components and nuclear displacements. The threshold on energy between two subsequent optimization steps was set to 10^{-7} Hartree; the thresholds on the root-mean-square of the gradient components and of the nuclear displacements were set to 3.0·10^{-4} Hartree bohr^{-1} and 1.2·10^{-3} bohr, respectively; those on the maximum components of the gradients and displacements were set to 4.5·10^{-4} Hartree bohr^{-1} and 1.8·10^{-3} bohr, respectively.

The specific surface energy γ (J/m^2) at a temperature T = 0 K was calculated as follows:[32]

$$\gamma = \lim_{n \to \infty} E_s(n) = \lim_{n \to \infty} \frac{E(n)_{slab} - nE_{bulk}}{2A} \quad (1)$$

where $E(n)$ is the energy of a n-layer slab; E_{bulk} is the energy of the bulk; A is the area of the surface unit cell; the factor 2 in the denominator accounts for the upper and lower surfaces of the slab model. $E_s(n)$ is thus the energy per unit area required for the formation of the surface from the bulk. As more layers are added in the calculation ($n \to \infty$), $E_s(n)$ will converge to the surface energy per unit area (γ).

The number of d_{hkl} layers to be considered in each slab, n, was set to values such that the relative difference between $E_s(n)$ and $E_s(n-1)$ is < 1%, in order to ensure a satisfactory convergence on surface energy and structure. In particular, within the adopted computational scheme, n is equal to 8, 4, 5, 8, 4, 4, 4 for the (010), (101), (111), (001), (110), (120) and (021) surfaces considered in this work (see Figures 1 and 2 and Figures S1-S5, Supporting Information). Then, the thickness of the converged (010), (101), (111), (001), (110), (120) and (021) slabs are $8d_{020}=40.96$, $4d_{101}=14.96$, $5d_{111}=17.55$, $8d_{002}=23.92$, $4d_{110}=17.32$, $4d_{120}=14.00$ and $4d_{021}=15.56$ Å, respectively; the optimized 2D cell parameters of the slabs are listed in Table 1. All of these converged slabs are charge neutral and contain 112 atoms; the center of inversion or a mirror plane parallel to the face was retained in the calculations, to ensure the dipole moment perpendicular to the slab is equal to zero.

Table 1. Optimized 2D cell parameters of the seven slabs under study.

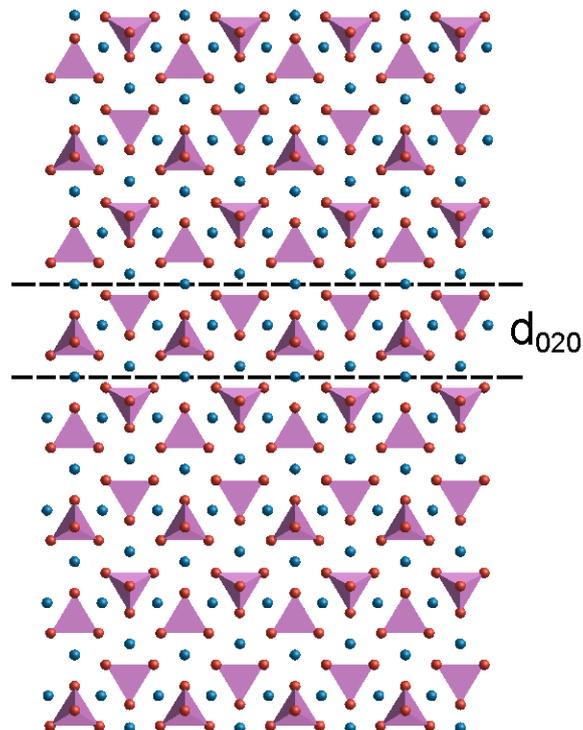|	a(Å)	b(Å)	a^b(°)	area(Å^2)
(010)	4.7947	6.0432	90.00	28.97
(101)	7.7449	10.2534	90.11	79.41
(111)	7.6837	11.1473	105.08	82.70
(001)	4.8055	10.1488	91.03	48.76
(110)	6.1046	11.0616	90.00	67.53
(120)	6.0087	13.9318	90.40	83.71
(021)	4.8276	15.6504	89.66	75.55

Figure 1. (010) surface viewed along [001]; d_{020} is the interplanar distance, i.e. the distance between adjacent 020 planes.
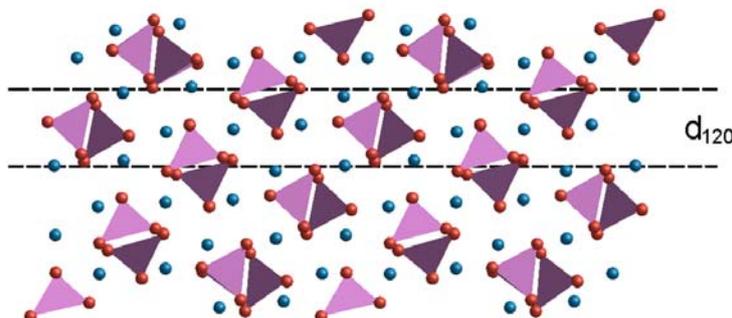

Figure 2. (120) surface viewed along [001]; d_{120} is the interplanar distance, i.e. the distance between adjacent 120 planes.

3. The structure of the forsterite surfaces

The experimental bulk crystal structure (space group *Pbnm*; a_0=4.7490, b_0=10.1985, c_0= 5.9792 Å[38]) was allowed to relax within the adopted computational scheme, giving a_0=4.7868, b_0=10.2552, c_0=6.0108 Å. The crystal was then cut taking inspiration from 'T Hart[39] who classified and studied the structures of the crystallographic forms of forsterite by applying the Periodic Bond Chain analysis (PBC) by Hartman and Perdok.[40-42] According to this analysis, the (010), (101), (111), (001), (110), (120) and (021) faces are classified as *F* (flat) faces, having at least two PBCs running inside the slices with thickness d_{hkl}. Therefore, they are the most important faces in naturally occurring crystals.

Let us analyse the surface structural modifications in vacuo at T = 0 K by taking the ideal bulk structure as a reference. In particular, the distortion of the SiO_4 tetrahedral units belonging to the first layer of the slab, i.e. that in contact with vacuum, can be used as a quantitative measure of how much the surfaces reconstruct.

Table 2 reports the values for the Si-O bond distances for both the bulk and the seven surfaces. Notably, the first layer of the (010), (111) and (001) slabs is made up by two independent tetrahedra, whereas in the case of the (101), (110), (120) and (021) slabs non-equivalent polyhedra are four. Two statistical indices can be adopted to summarise the effect of atomic relaxation: the average Si-O bond distance per tetrahedron, <Si-O> [Å], and the difference between the maximum and the minimum bond distance per tetrahedron, Δ [Å].

The average Si-O distance in forsterite is 1.6516 Å. Out of the 22 symmetry independent surface tetrahedra belonging to the seven slabs, 15 have average distances lying within 0.01 Å from the bulk value. The 7 average deviations from the bulk larger than 0.01 Å are found in the cases of (111) (both tetrahedra, 1.6684 and 1.6647 Å), (001) (1.6651 Å), (101) (1.6646 Å), (110) (2 tetrahedra, 1.6793 Å and 1.6405 Å), and (120) (1.6667 Å). At the other extreme, all the tetrahedra of both (010) and (021) slabs have average Si-O distances differing by only ±0.1 % from the bulk value (absolute difference ≤ 0.003 Å).

The difference between the maximum and minimum Si-O distances in forsterite is 0.0446 Å. Only in two cases (0.0301 Å in (001), 0.0381 Å in (110)) this deviation Δ is smaller in the slabs than in the bulk; in all other cases it is larger, indicating the preference of tetrahedra at surfaces to increase their degree of distortion. The maximum Δ is found in the case of (101), 0.1624 Å. The marked distortion of the tetrahedra comes along with large variations of the Mg-O distances and is due to a significant structural rearrangement suffered by the surfaces in order to increase their atomic density and reach a more stable configuration. Having a look at the single Si-O distance values, we note that the longest Si-O distance (1.7376 Å) is observed for the (110) slab, whereas the shortest one (1.5679 Å) for the (101) slab.

The relaxed structures of the (010) and (120) surfaces (the most stable ones, see Section 4) are shown in Figures 1 and 2; structures for the other five crystallographic orientations are reported in the Supporting Information.

Upon inspection of Figures 1, 2 and S1-S5, and of the data reported in Table 2 and commented in the previous paragraphs, it is worth noting that the face displaying the smallest surface relaxation is the (010). In this case the first d_{020} layer suffers an extremely slight structural modification, as expected on the basis of experimental findings.[43] Furthermore, such a weak relaxation is associated with the lowest surface energy value (see Section 4).

Table 2. Optimized Si-O distances [Å] of forsterite and of its (010), (101), (111), (001), (110), (120) and (021) surfaces at 0 K. Surface data are reported for the SiO$_4$ tetrahedra lying on the first layer. Each column stands for a symmetry independent tetrahedron: they are two in (010), (111) and (001) surfaces, four in the other surfaces. <Si-O> [Å] is the average Si-O bond length per tetrahedron; Δ [Å] is the difference between the maximum and minimum Si-O distance values. The relative % difference of <Si-O> and Δ with respect to the bulk is reported.

	Bulk	(101)			
Si-O	1.6282	1.5940	1.5679	1.6261	1.6247
	1.6527	1.6232	1.6626	1.6453	1.6414
	1.6527	1.6878	1.6974	1.6560	1.6597
	1.6728	1.7079	1.7303	1.7061	1.6784
<Si-O>	1.6516	1.6532	1.6646	1.6584	1.6511
		+0.1	*+0.8*	*+0.4*	*0.0*

Δ	0.0446		0.1139	0.1624	0.0800	0.0537
			+155.4	*+264.1*	*+79.4*	*+20.4*
	(010)			**(110)**		
Si-O	1.6110	1.6272	1.5972	1.6438	1.6037	1.6131
	1.6437	1.6399	1.6971	1.6438	1.6037	1.6476
	1.6437	1.6399	1.7114	1.6716	1.6168	1.6476
	1.6967	1.7015	1.7114	1.6819	1.7376	1.6750
<Si-O>	1.6488	1.6521	1.6793	1.6603	1.6405	1.6458
	-0.2	*0.0*	*+1.7*	*+0.5*	*-0.7*	*-0.4*
Δ	0.0857	0.0743	0.1142	0.0381	0.1339	0.0619
	+92.2	*+66.6*	*+156.1*	*-14.6*	*+200.2*	*+38.8*
	(111)			**(120)**		
Si-O	1.6131	1.5877	1.5855	1.5916	1.6206	1.6373
	1.6622	1.6488	1.6513	1.6452	1.6526	1.6399
	1.6813	1.7099	1.7143	1.6615	1.6644	1.6549
	1.7170	1.7122	1.7156	1.6918	1.7058	1.7095
<Si-O>	1.6684	1.6647	1.6667	1.6475	1.6609	1.6604
	+1.0	*+0.8*	*+0.9*	*-0.2*	*+0.6*	*+0.5*
Δ	0.1039	0.1245	0.1301	0.1002	0.0852	0.0722
	+133.0	*+179.1*	*+191.7*	*+124.7*	*+91.0*	*+61.9*
	(001)			**(021)**		
Si-O	1.6179	1.6298	1.6053	1.6162	1.6112	1.6331
	1.6468	1.6362	1.6269	1.6428	1.6366	1.6392
	1.6684	1.6564	1.6625	1.6499	1.6501	1.6533
	1.7274	1.6599	1.7057	1.7054	1.7086	1.6895
<Si-O>	1.6651	1.6456	1.6501	1.6536	1.6516	1.6538
	+0.8	*-0.4*	*-0.1*	*+0.1*	*0.0*	*+0.1*
Δ	0.1095	0.0301	0.1004	0.0892	0.0974	0.0564
	+145.5	*-32.5*	*+125.1*	*+100.0*	*+118.4*	*+26.5*

4. The surface energies and the equilibrium shape at 0 K of forsterite

Table 3 lists the surface energies γ of the seven crystallographic forms of forsterite analyzed in this work; they refer to the converged thick slabs discussed in Section 2. The faces with the lowest and highest surface energy result to be the {010} and {110}, respectively. Then, the stability order of the surfaces is (010) < (120) < (001) < (101) < (111) < (021) < (110).

As a comparison, Table 3 reports the surface energy values previously calculated by Watson et al.,[13] de Leeuw et al.,[12] and Garcia-Gil et al.;[14] de Leeuw et al.[12] did not provide a surface energy value for the (120) face, therefore it has been calculated in this work by using their force field. There is a good agreement between our values and those obtained at an empirical level by Watson

et al.[13] and de Leeuw et al.[12] for the surfaces in vacuum. As concerns de Leeuw et al.,[12] the highest difference (-12.8%) is observed for the (120) face, while the lowest one (1.6%) is related to the (111) face. Instead, as concerns Watson et al.,[13] the highest (-12.8%) and lowest (-1.6%) differences are observed for the (120) and (101) faces, respectively. These evidences suggest that the force field employed by Watson et al.[13] and de Leeuw et al.[12] for describing atomic interactions in forsterite could be an effective starting point to study the surfaces of this mineral.

Here, it is worth noting that Watson et al.[13] calculated the surface energy for three different terminations of the (110) face: (i) the surface termination with the highest surface energy (2.28 J/m^2) corresponds to the one considered in our work (2.18 J/m^2); (ii) the surface termination with the lowest surface energy (1.70 J/m^2), that is the more stable surface termination, was not taken into account in our work. Then, for sake of comparison with our data, in the following we only discuss the case (i), but it is important to underline that the more stable surface termination of the (110) face is that reported in the paper by Watson et al.[13] Moreover, due to the very good agreement between our results and those from Watson et al.,[13] it is likely that the energy of most stable (110) termination if calculated by our approach would be very similar to that of Watson et al.[13]

Finally, the work recently published by Garcia-Gil et al.[14] reports a (010) surface energy value (1.20 J/m^2) that is very close to the one estimated in the present study (1.22 J/m^2). This is not surprising, because these authors performed periodic first principles DFT calculations with the PBE functional.[25,44] Unfortunately, they studied the adsorption of H atoms on the (010) surface only; as a consequence, other crystal faces were disregarded.

By applying the Gibbs–Wulff's theorem[45] and considering our surface energy values listed in Table 3, we were able to draw the equilibrium shape (ES) of a forsterite crystal in vacuum at 0 K (Figure 3a). As a comparison, we also drew the ESs by using surface energy values calculated by Watson et al.[13] (Figure 3b) and de Leeuw et al.[12] (Figure 3c).

In order to analyze quantitatively the differences occurring between the ES presented in this work and those published in previous studies, we computed the morphological relevance index MRI for all the {hkl} forms; it is defined as the percent ratio between the total area of the faces belonging to a given {hkl} form and the total surface area of the crystal. Values are reported in Table 4. The morphological relevance order for the ES proposed in this study (Figure 3a) is {120}, {010}, {001}, {101}, {111} and {021}. A quite similar ES is observed when considering the Watson et al.'s data[13] (Figure 3b), with the following morphological relevance order: {010}, {120}, {001}, {111}, {101} and {021}. The main difference is the inverted ranking of the {010} and {120} forms, and of the {101} and {111} forms. Note that absolute differences between MRI values can be as large as 12.0 in the case of (120); the smallest deviation is 3.4 for (021).

Finally, we consider the ES obtained by de Leeuw et al.[12] (Figure 3c); it turns to be quite similar to the one determined in this work. The morphological relevance order is the following: {111}, {120}, {010}, {001}, {101} and {021}. The main difference is the ranking of the {111} form, 1st instead of 5th. Only 3 out of 7 forms have absolute deviations larger than 3.5: {111} with -17.4, {120} with 11.5 and {101} with 8.2.

Unfortunately, the comparison between theoretical and real ESs of olivine is not possible for the following two main reasons: (i) the olivine does not grow in the vacuum, but it is found in magmatic and metamorphic rocks. A correct evaluation of the ES requires the knowledge of the free energy of the olivine/growth medium interfaces; (ii) the real morphologies are always obtained at T > 0 K, whereas our calculations were performed at T = 0 K. For a correct comparison between theoretical and real ESs, the knowledge of how the temperature affects the interface free energy values, and hence the crystal ES, is fundamental. This implies the ability to calculate the vibrational and configurational entropy of the different olivine interfaces at the temperature of interest.

Table 3. Surface energies γ at 0 K [J/m^2] of the main crystal faces of forsterite. Percentage variations Δ(%) with respect to previous studies are reported.

face	this work	Watson et al.[13]	Δ(%)	de Leeuw et al.[12]	Δ(%)	Garcia-Gil et al.[14]	Δ(%)
(010)	1.22	1.28	-4.7	1.28	-4.7	1.20	1.7
(101)	1.78	1.81	-1.6	1.88	-5.3	-	-
(111)	1.84	1.80	2.2	1.81	1.6	-	-
(001)	1.78	1.61	10.1	1.74	2.3	-	-
(110)	2.18	2.28	-4.4	1.96	11.2	-	-
(120)	1.36	1.56	-12.8	1.56^a	-12.8	-	-
(021)	1.90	1.95	-2.6	1.94	-2.1	-	-

^{a} Calculated in this work by using the force field of de Leeuw et al.[12]

Table 4. Morphological relevance index MRI at 0 K [%] of the main crystal faces of forsterite. Absolute variations Δ with respect to previous studies are reported.

face	this work	Watson et al.[13]	Δ	de Leeuw et al.[12]	Δ
(010)	21.7	25.9	-4.2	24.9	-3.2
(101)	12.2	8.6	3.6	4.0	8.2
(111)	8.2	19.1	-10.9	25.6	-17.4
(001)	15.8	19.7	-3.9	16.2	-0.4
(110)	0.0	0.0	0.0	0.0	0.0
(120)	37.0	25.0	12.0	25.5^a	11.5
(021)	5.1	1.7	3.4	3.8	1.3

^{a} Calculated in this work by using the force field of de Leeuw et al.[12]
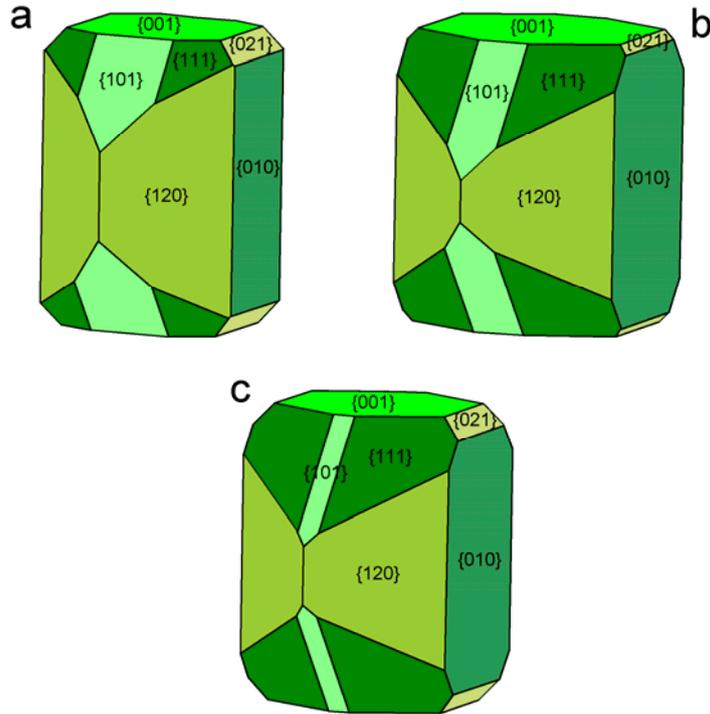
Figure 3. Equilibrium shape (ES) of forsterite at 0 K: (a) ES obtained with surface energy values from this study; (b) ES obtained with the surface energy values calculated by Watson et al.;[13] (c) ES obtained with the surface energies calculated by de Leeuw et al.[12]

5. Some considerations about the shape and genesis of olivine included in diamond

The importance of studying the surfaces and shape of olivine is elucidated in this paragraph, where it is shown how a detailed analysis of the crystal shape can reveal fundamental information to understand the genesis of mineral inclusions in diamond. Indeed, the shape of olivine included in diamond is very different from that of olivine crystals not entrapped inside the diamond and from the equilibrium one determined in this work. Therefore, in the light of the results above reported and discussed, in this section we try to explain such a morphological difference.

Diamond inclusions (DIs) are divided into three groups: *protogenetic*, *syngenetic* and *epigenetic*.[46] DIs are classified as protogenetic when they formed before the encapsulation by the host diamond, whereas they are considered syngenetic when the inclusion and its host diamond formed at the same time and by the same genetic processes. Both groups play a key role in the study of diamond formation processes, contrary to epigenetic phases, which are secondary minerals, usually associated with crustal processes, and atypical with respect to the primary minerals in mantle xenoliths.

Such distinction is important, because in the case of syngenesis any geological information extracted from the inclusion (e.g., pressure and temperature of formation, geochemical

12

environment, age) would also unequivocally apply to its host diamond. On the other hand, a protogenetic inclusion would record conditions that existed before its encapsulation; the corresponding time range might span from short to very long geological timescales. In the latter case the protogenetic inclusion could be completely unrelated to the formation of host diamond. Demonstrably protogenetic inclusions would support models of diamond formation involving fluxes of C-bearing fluids through pre-existing mantle rocks and could help explain occurrences of isotopically different inclusions in the same generation of diamond (e.g., Thomassot et al.[47]).

Distinguishing between syngenesis and protogenesis is as crucial as extremely difficult and controversial, as demonstrated by Taylor et al.[48] The most common observation used to deduce syngenesis is the imposition of the host diamond morphology on the DI (e.g., Meyer,[46,49] Pearson and Shirey,[50] Harris[51]). Concerning this argument, it is worth noting that the morphology of orthorhombic minerals (such as olivine and enstatite) included in diamond (with its well known cubic symmetry) is usually described as "cubo-octahedral".[11,48,52] In order to explain such an "exotic" morphology, as reported by Taylor et al.,[48] a "... greater *form energy* of diamond (also named *crystalloblastic force* of diamond faces)" is invoked, "that thereby imposes its morphology upon the inclusion, *during mutual growth*". In the present study we will show that it is not necessary to resort to a rather undefined force to explain the shape of DIs; indeed, the observed morphology of olivine inclusions may be interpreted by only means of the crystallographic forms of the orthorhombic system, with no recourse to the crystallographic forms of diamond cubic system.

Another significant contribution to the syngenesis *vs* protogenesis debate derives from the observation that some DIs occur in a specific orientation relationship with respect to diamond, which can be considered as an evidence in favor of epitaxial growth of the DI above the diamond or vice versa, and hence of syngenesis.[46,49,50,53-59] The first findings concerning possible epitaxial growth were those by Mitchell and Giardini,[59] who reported oriented inclusions of olivine in diamonds: the (010) face of olivine was parallel to the (111) one of diamond and the zone [101] of olivine was parallel to that [101] of diamond. Wiggers de Vries et al.[60] recently reported on electron backscatter diffraction observations, showing that the <100> crystallographic directions of diamond were parallel to the <100> directions of their chromite inclusions. Instead, in a very recent work by our research group,[61] the crystallographic orientations of forty-seven olivines incorporated in twenty-one diamonds from Udachnaya kimberlite (Siberia) were analyzed and, at variance with the finding by Mitchell and Giardini,[59] no preferential orientation was observed between olivine and diamond. On this basis, a protogenetic origin was hypothesized for these olivines. In the present study we will discuss in more detail the mechanism of formation of DIs initially proposed by

Nestola et al.[61] Such mechanism is able to explain the somewhat different morphology of olivine crystals included in diamond with respect to that of crystals outside the diamond host.

As pointed out above, the morphology of olivine included in diamond (i.e. orthorhombic against cubic symmetry, respectively) is usually described as "cubo-octahedral".[11,48,52] Indeed, the crystallographic forms of an orthorhombic mineral are pinacoid ({100}, {010} and {001}), orthorhombic prism ({hk0}, {h0l} and {0kl}) and orthorhombic bipyramid ({hkl}). Therefore, it is evident that the cube and octahedra cannot be used to properly describe the morphology of olivine; from a crystallographic point of view, referring to olivine morphology as "cubo-octahedral" is wrong and can generate ambiguities in the process of interpreting the genesis of an inclusion.

Using an example, we will now show that the so called "cubo-octahedral" shape of olivine inclusions is nothing more than a consequence of the association of orthorhombic forms. Figure 4 depicts a diamond showing the {100}-cube and {111}-octahedra forms, along with an olivine crystal having the pinacoids ({100}, {010} and {001}) and the bipyramid {495}; the a≡[100], b≡[010] and c≡[001] axis of olivine are parallel to the [100], [010] and [001] ones of the diamond, respectively. Interestingly, the (495) face of olivine is a vicinal one, which results to be parallel to the (111) face of the diamond; this can make very difficult to distinguish olivine from diamond by only observing their morphology: the shape of olivine may be equal to that of diamond, even if the forms making up the two crystals are completely different. The simple example reported here is meant to explain the origin of the ambiguities in describing the olivine morphology; it is worth stressing that also in other cases of mutual orientation between olivine and diamond it is possible to identify a vicinal face of olivine having the same orientation of the (111) of diamond.
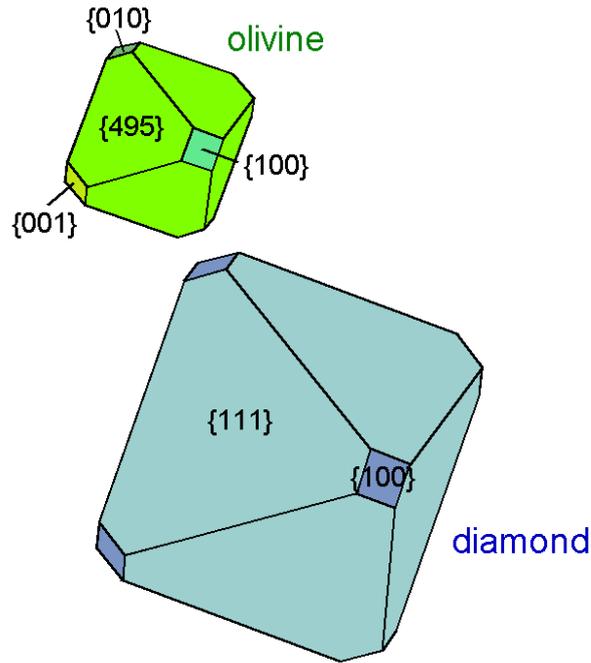
Figure 4. Diamond and olivine crystals showing the same shape, but different crystallographic forms. The a≡[100], b≡[010] and c≡[001] axes of olivine are parallel to the [100], [010] and [001] ones of diamond, respectively.

In what follows, by taking into account our analysis on the olivine morphology and our previous study on the orientation of olivines included in diamonds from Udachnaya,[61] some considerations about the genesis of the DIs are reported.

As stated above, the most common observation used to deduce syngenesis is the imposition of the host diamond morphology on the DI (e.g., Meyer,[46,49] Pearson and Shirey,[50] Harris[51]). However, as demonstrated by Taylor et al.,[48] some peridotitic garnet inclusions (the garnet is a silicate mineral and peridotite is a rock composed mainly by olivine), having morphology imposed by the host diamond, clearly show a Rare Earth Element (REE) pattern typical of garnets found worldwide and not included in diamonds. Taylor et al.[48] stated that this observation is consistent with a protogenetic nature, at least for peridotitic garnets. Similar conclusions were drawn by Thomassot et al.,[47] who investigated isotopes of sulfide inclusions in diamonds, and Spetsius et al.,[62] who analysed inclusions found in zircons extracted from diamonds.

In order to conciliate the geochemical observations on the REE pattern with the morphological ones, we propose the following mechanism for explaining the genesis of the DIs; this mechanism, briefly described in the paper by Nestola et al.,[61] is here exemplified by considering the formation of an olivine DI, but it can be easily generalized to a DI of any kind. Let us suppose that a diamond nucleates at time t_0 in a peridotitic rock (Figure 5), i.e. when a C-H-O fluid becomes supersaturated with respect to the diamond phase. Then, the diamond grows and

gains space at the expense of olivine, which dissolves at the diamond/olivine interface (Figure 5, time t_1). At a certain point of its growth history (Figure 5, time t_2), the diamond begins to include a piece of olivine and, at the same time, the diamond/olivine interface is adjusted throughout transport of matter by means of interface diffusion; in this way the diamond/olivine interface strain energy is minimized and the olivine morphology is modified. Finally, at time t_3 (Figure 5), the diamond fully envelops the olivine, which has now a completely different morphology with respect to the external crystals; in parallel, the original geochemical fingerprint is left unchanged, as in the case of the peridotitic garnet inclusions described by Taylor et al.[48] As reported by Nestola et al.,[61] the result of the proposed mechanism is that, if the diamond growth is fast enough and the process temperature is not high enough to allow chemical and isotopic re-equilibration, then the DI might record age and P-T conditions of formation that could be older than those of the host diamond.

A strong proof in favor of this model is the finding of multiple inclusions of olivine within the same diamond showing a similar orientation. Indeed, no more than three sets of iso-oriented olivines were found within single diamond.[61] This could suggest that the probability to incorporate more than three original olivine monocrystals in a growing diamond is very low and, as a consequence, diamond should grow between adjacent grains of olivine.

Some interesting consequences derive from the proposed diamond growth mechanism:

(i)   the morphology of the DI cannot be considered as an evidence of syngenesis;

(ii)   the DI preserves the original orientation of the crystal from which it is detached;

(iii)   if the crystal morphology is modified, but the DI does not show a preferential orientation with respect to the diamond (i.e., no epitaxial relationship between diamond and DI), then it is highly likely that the growth mechanism we propose is correct. This implies that the *bulk* of the DI is protogenetic, while its *shape* is syngenetic;

(iv)   if the crystal morphology is modified and the DI shows a preferential orientation with respect to the diamond (i.e., epitaxial relationship between diamond and DI), then it is highly likely that the DI nucleated above a diamond face or vice versa. Therefore, both the *bulk* and *shape* of the DI are syngenetic.

Up to now we have discussed the case of a well-shaped DI, but the majority of them display a rounded shape, which is likely due to the development of a great number of vicinal faces during the process of diamond growth. As a matter of fact, some orientations of olivine are not able to produce the "cubo-octahedral"-like shape discussed above. Then, in order to reduce the interface strain energy, the shape of olivine could adapt to diamond by realizing an envelope of vicinal faces that mime a rounded morphology. Otherwise stated, in some cases the olivine has a crystallographic orientation that does not allow the development of a simple shape formed by a limited number of

vicinal faces; a complex morphology composed by a large number of crystallographic forms is developed instead, to minimize the strain energy of diamond/olivine interface. However, further studies are required to develop and validate this hypothesis. In particular, a detailed crystallographic analysis should be performed for determining the forms of the olivine included in diamond.
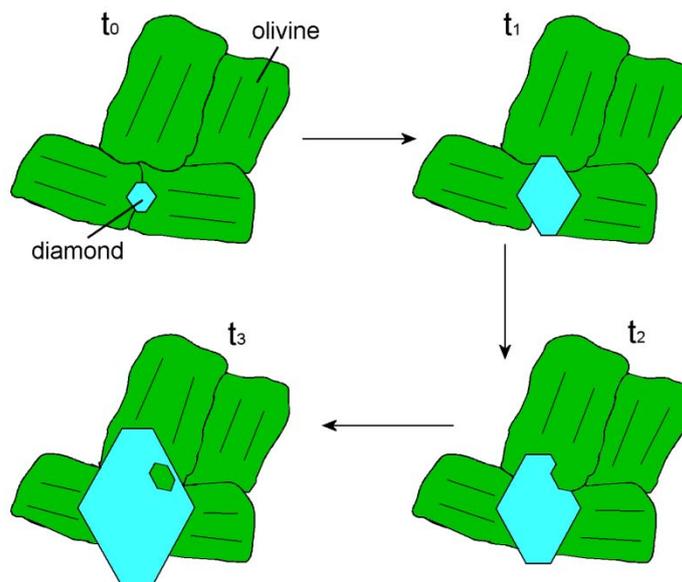

Figure 5. Schematic drawing representing the formation of an olivine inclusion in diamond.

6. Conclusions

In this work, we have presented an accurate *ab initio* study of the structure and surface energy at 0 K of the low-index (010), (101), (111), (001), (110), (120) and (021) forsterite faces, by using for the first time, at the best of our knowledge, the hybrid Hartree-Fock/Density Functional B3LYP Hamiltonian and a localized all-electron Gaussian-type basis set. Furthermore, these results have been combined with experimental evidences to develop some considerations about the shape and genesis of olivine included in diamond, which show a very different crystal morphology with respect to that of olivine crystals not entrapped inside the diamond.

     We can summarize our results in the following points:

(i)   the face displaying the smallest surface relaxation is the (010): the first d_{020} layer suffers an extremely slight structural modification and, as expected, such a weak relaxation is associated with the lowest surface energy value.

(ii) According to the surface energy values, the stability order of the forsterite faces is (010) < (120) < (001) < (101) < (111) < (021) < (110).

(iii) The equilibrium shape (ES) of a forsterite crystal has been drawn by using our surface energy values. It results to be quite similar to the one determined at empirical level by Watson et al.[13] and de Leeuw et al.[12] This suggests that the force field employed by these authors could be used as a starting point for fitting a new interatomic potential for studying the chemical reactions occurring at the olivine/water interfaces.

(iv) As an example of the importance of understanding the surfaces and shape of olivine and in order to contribute to the syngenesis *vs* protogenesis debate, we have discussed the peculiar crystal morphology of olivine included in diamond (DI). First, we have showed that the observed "cube-octahedral" shape of olivine in diamond is actually a combination of orthorhombic bipyramid (i.e., {495}) and pinacoids. This implies that the shape of olivine may be equal to that of diamond, even if the forms making up the two crystals are completely different. Second, we have demonstrated that the morphology of the DI cannot be considered as an evidence of syngenesis. In particular, if the crystal morphology is modified, but the DI does not show a preferential orientation with respect to the diamond, the *bulk* of the DI is protogenetic, while its *shape* is syngenetic.

AUTHOR INFORMATION
Corresponding author
*(M.B) E-mail: marco.bruno@unito.it. Phone: (39) 0116705126. Fax: (39) 0116705128.

SUPPORTING INFORMATION AVAILABLE. Figures S1-S5: optimized structures of the (101), (111), (001), (110) and (021) faces of forsterite. This material is available free of charge via the Internet at http://pubs.acs.org.

REFERENCES

(1) Dana, E.S. *A Textbook of Mineralogy*; John Wiley: New York, USA, 1941.

(2) Hiesinger, H.; Helbert, J. MERTIS Co-I Team, The Mercury Radiometer and Thermal Infrared Spectrometer (MERTIS) for the Bepi Colombo mission. *Planet. Space Sci.* **2010**, *58*, 144-165.

(3) Antretter, M.; Fuller, M. Paleomagnetism and Rock Magnetism of Martian Meteorite ALH 84001. *Phys. Chem. Earth* **2002**, *27*, 1299-1303.

(4) Tarduno, J.A.; Cottrell, R.D.; Smirnov, A.V. The Paleomagnetism of Single Silicate Crystals: Recording Geomagnetic Feld Strength During Mixed Polarity Intervals, Superchrons, and Inner Core Growth. *Rev. Geophys.* **2006**, *41*, RG1002.

(5) Hwang, S.L.; Yui, T.F.; Chu, H.T.; Shen, P.; Iizuka, Y.; Yang, H.Y.; Yang, J.; Xu, Z. Hematite and Magnetite Precipitates in Olivine from the Sulu Peridotite: a Result of Dehyhrogenation-Oxidation Reaction of Mantle Olivine? *Am. Mineral.* **2008**, *93*, 1051-1060.

(6) Belley, F.; Ferré, E.C.; Martín-Hernández, F.; Jackson, M.J.; Dyar, M.D.; Catlos, E.J. The Magnetic Properties of Natural and Synthetic $(Fe_x, Mg_{1-x})_2 SiO_4$ Olivines. *Earth Planet. Sci. Lett.* **2009**, *284*, 516-526.

(7) Evans, B.W.; Hattori, K.; Baronnet, A. Serpentinite: What, Why, Where? *Elements* **2013**, *9*, 99-106.

(8) Power, I.M.; Wilson, S.A.; Dipple, G.M. Serpentinite Carbonation for CO_2 Sequestration. *Elements* **2013**, *9*, 115-121.

(9) McCollom, T.M.; Seewald, J. Serpentinites, Hydrogen, and Life. *Elements* **2013**, *9*, 129-134.

(10) Müntener, O. Serpentine and Serpentinization: A Link between Planet Formation and Life. *Geology* **2010**, *38*, 959-960.

(11) Stachel, T.; Harris, J.W. The Origin of Cratonic Diamonds – Constraints from Mineral Inclusions. *Ore Geol. Rev.* **2008**, *34*, 5-32.

(12) de Leeuw, N.H.; Parker, S.C.; Catlow, C.R.A.; Price, G.D. Modelling the Effect of Water on the Surface Structure and Stability of Forsterite. *Phys. Chem. Minerals* **2000**, *27*, 332-341.

(13) Watson, G.W.; Oliver, P.M.; Parker, S.C. Computer Simulation of the Structure and Stability of Forsterite Surfaces. *Phys. Chem. Minerals* **1997**, *25*, 70-78.

(14) Garcia-Gil, S.; Teillet-Billy, D.; Rougeau, N.; Sidis, V. H Atom Adsorption on a Silicate Surface: The (010) Surface of Forsterite *J. Phys. Chem. C* **2013**, *117*, 12612-12621.

(15) Downing, C.A.; Ahmady, B.; Catlow C.R.A.; de Leeuw N.H. The interaction of hydrogen with the {010} surfaces of Mg and Fe olivine as models for interstellar dust grains: a density functional theory study. *Phil. Trans. R. Soc. A* **2013**, *371*, 20110592.

(16) King, H.E.; Stimpfl, M.; Deymier, P.; Drake, M.J.; Catlow, C.R.A.; Putnis, A.; de Leeuw, N.H. Computer Simulations of Water Interactions with Low-Coordinated Forsterite Surface Sites: Implications for the Origin of Water in the Inner Solar System. *Earth Planet. Sci. Lett.* **2010**, *300*, 11-18.

(17) Goumans, T.P.M.; Catlow, C.R.A.; Brown, W.A. Formation of H_2 on an Olivine Surface: a Computational Study. *Mon. Not. R. Astron. Soc.* **2009**, *393*, 1403-1407.

(18) Muralidharan, K.; Deymier, P.; Stimpfl, M.; de Leeuw, N.H.; Drake, M.J. Origin of Water in the Inner Solar System: A kinetic Monte Carlo Study of Water Adsorption on Forsterite. *Icarus* **2008**, *198*, 400-407.

(19) de Leeuw, N.H. Density Functional Theory Calculations of Hydrogen-Containing Defects in Forsterite, Periclase, and Alpha-Quartz. *J. Phys. Chem. B* **2001**, *105*, 9747-9754.

(20) Stephens, P.J.; Devlin, F.J.; Chabalowski, C.F.; Frisch, M.J. Ab Initio Calculation of Vibrational Absorption and Circular Dichroism Spectra Using Density Functional Force Fields. *J. Phys. Chem.* **1994**, *98*, 11623-11627.

(21) Becke, A.D. Density-Functional Thermochemistry. III. The Role of Exact Exchange. *J. Chem. Phys.* **1993**, *98*, 5648-5652.

(22) Lee, C.; Yang, W.; Parr, R.G. Development of the Colle-Salvetti Correlation Energy Formula into a Functional of the Electron Density. *Phys. Rev. B* **1988**, *37*, 785-789.

(23) De La Pierre, M.; Bruno, M.; Manfredotti, C.; Nestola, F.; Prencipe, M.; Manfredotti, C. The (100), (110) and (111) Surfaces of Diamond: an Ab Initio B3LYP Study. *Molecular Physics* **2013**, DOI 10.1080/00268976.2013.829250.

(24) Noël, Y.; De La Pierre, M.; Maschio, L.; Rérat, M.; Zicovich-Wilson, C.M.; Dovesi, R. Electronic Structure, Dielectric Properties and Infrared Vibrational Spectrum of Fayalite: an Ab Initio Simulation with an All-Electron Gaussian Basis Set and the B3LYP Functional. *Int. J. Quantum Chem.* **2012**, *112*, 2098-2108.

(25) De La Pierre, M.; Orlando, R.; Maschio, L.; Doll, K.; Ugliengo, P.; Dovesi, R. Performance of Six Functionals (LDA, PBE, PBESOL, B3LYP, PBE0, and WC1LYP) in the Simulation of Vibrational and Dielectric Properties of Crystalline Compounds. The Case of Forsterite Mg_2SiO_4. *J. Comput. Chem.* **2011**, *32*, 1775-1784.

(26) Demichelis, R.; Civalleri, B.; Ferrabone, M.; Dovesi, R. On the Performance of Eleven DFT Functionals in the Description of the Vibrational Properties of Aluminosilicates. *Int. J. Quantum Chem.* **2010**, *110*, 406-415.

(27) Ottonello, G.; Civalleri, B.; Ganguly, J.; Vetuschi Zuccolini, M.; Noël, Y. Thermophysical Properties of the Apha-Beta-Gamma Polymorphs of Mg_2SiO_4: a Computational Study. *Phys. Chem. Miner.* **2009**, *36*, 87-106.

(28) Noël, Y.; Catti, M.; D'Arco, P.; Dovesi, R. The Vibrational Frequencies of Forsterite Mg_2SiO_4: an All-Electron Ab Initio Study with the CRYSTAL Code. *Phys. Chem. Miner.* **2006**, *33*, 383-393.

(29) Dovesi, R.; Saunders, V.R.; Roetti, C.; Orlando, R.; Zicovich-Wilson, C.M.; Pascale, F.; Civalleri, B.; Doll, K.; Harrison, N.M.; Bush, I.J.; D'Arco, Ph.; Llunell, M. *CRYSTAL09 User's Manual*; University of Torino: Torino, Italy, 2009.

(30) Dovesi, R.; Orlando, R.; Civalleri, B.; Roetti, C.; Saunders, V.R.; Zicovich-Wilson, C.M. CRYSTAL: a Computational Tool for the Ab Initio Study of the Electronic Properties of Crystals. *Z. Kristallogr.* **2005**, *220*, 571-573.

(31) Pisani, C.; Dovesi, R.; Roetti, C. *Hartree-Fock Ab-Initio Treatment of Crystalline Systems, Lecture Notes in Chemistry*; Springer: Berlin, Heidelberg, New York, 1988.

(32) Dovesi, R.; Civalleri, B.; Orlando, R.; Roetti, C.; Saunders, V.R. In *Reviews in Computational Chemistry*; Lipkowitz, B.K., Larter, R., Cundari, T.R., Eds.; John Wiley & Sons, Inc.: New York, 2005; pp 1-125.

(33) Becke, A.D. Density-Functional Exchange-Energy Approximation with Correct Asymptotic Behavior. *Phys. Rev. A* **1988**, *38*, 3098-3100.

(34) Monkhrost, H.J.; Pack, J.D. Special Points for Brillouin-Zone Integration. *Phys. Rev. B* **1976**, *13*, 5188-5192.

(35) Civalleri, B.; D'Arco, Ph.; Orlando, R.; Saunders, V.R.; Dovesi, R. Hartree-Fock Geometry Optimisation of Periodic Systems with the CRYSTAL Code. *Chem. Phys. Lett.* **2001**, *348*, 131-138.

(36) Doll, K. Implementation of Analytical Hartree-Fock Gradients for Periodic Systems. *Comp. Phys. Commun.* **2001**, *137*, 74-88.

(37) Doll, K.; Saunders, V.R.; Harrison, N.M. Analytical Hartree-Fock Gradients for Periodic Systems. *Int. J. Quantum. Chem.* **2001**, *82*, 1-13.

(38) Bostrom, D. Single-Crystal X-ray Diffraction Studies of Synthetic Ni-Mg Olivine Solid Solution. *Am. Mineral.* **1987**, *72*, 965-972.

(39) 'T Hart, J. The Structural Morphology of Olivine; I, A Qualitative Derivation. *Can. Mineral.* **1978**, *16*, 175-186.

(40) Hartman, P.; Perdok, W.G. On the Relations between Structure and Morphology of Crystals. I. *Acta Cryst.* **1955**, *8*, 49-52.

(41) Hartman, P.; Perdok, W.G. On the Relations between Structure and Morphology of Crystals. II. *Acta Cryst.* **1955**, *8*, 521-524.

(42) Hartman, P.; Perdok, W.G. On the Relations between Structure and Morphology of Crystals. III. *Acta Cryst.* **1955**, *8*, 525-529.

(43) Lemelle, L.; Abel, F.; Cohen, C.; Guyot, F. Study of the (010) Olivine Surface by Rutherford Backscattering Spectrometry in Channeling Geometry. *Am. Mineral.* **2002**, *87*, 327-332.

(44) Perdew, J.P.; Burke, K.; Ernzerhof, M. Generalized Gradient Approximation Made Simple. *Phys. Rev. Lett.* **1996**, *77*, 3865-3868.

(45) Wulff, G. Zur Frage der Geschwindigkeit des Wachstums und der Auflosung der Krystallflachen. *Z. Kristallogr. Kristallgeom.* **1901**, *34*, 949.

(46) Meyer, H.O.A. In *Mantle Xenoliths*; Nixon, P.H., Ed.; John Wiley & Sons: Chichester, 1987; pp 501-522.

(47) Thomassot, E.; Cartigny, P.; Harris, J.W.; Lorand, J.P.; Rollion-Bard, C.; Chaussidon, M. Metasomatic Diamond Growth: a Multi-Isotope Study (^{13}C, ^{15}N, ^{33}S, ^{34}S) of Sulphide Inclusions and their Host Diamonds from Jwaneng (Botswana). *Earth Planet. Sci. Lett.* **2009**, *282*, 79-90.

(48) Taylor, L.A.; Anand, M.; Promprated, P. Diamonds and their Inclusions: are the Criteria for Syngenesis Valid? *Proceedings of the 8th International Kimberlite Conference* **2003**, *1*, 1-5.

(49) Meyer, H.O.A. Genesis of Diamond: a Mantle Saga. *Am. Mineral.* **1985**, *70*, 344-355.

(50) Pearson, D.G.; Shirey, S.B. In *Application of Radiogenic Isotopes to Ore Deposit Research and Exploration, Reviews in Economic Geology*; Lambert, D.D., Ruiz, J., Eds.; Society of Economic Geologists: Littleton CO, Denver, 1999; pp 143-172.

(51) Harris, J.W. The Recognition of Diamond Inclusions. Part 1: Syngenetic Mineral Inclusions. *Ind. Diam. Rev.* **1968**, *28*, 402-410.

(52) Nestola, F.; Nimis, P.; Ziberna, L.; Longo, M.; Marzoli, A.; Harris, J.W.; Manghnani, M.H.; Fedortchouk, Y. First Crystal-Structure Determination of Olivine in Diamond: Composition and Implications for Provenance in the Earth's mantle. *Earth Planet. Sci. Lett.* **2011**, *305*, 249-255.

(53) Bulanova, G.P. The Formation of Diamond. *J. Geochem. Explor.* **1995**, *53*, 1-23.

(54) Leeder, O.; Thomas, R.; Klemm, W. *Einschlusse in Mineralien*; VEB Deutscher Verlag fur Grunstoffenindustrie: Leipzig, Germany, 1987.

(55) Harris, J.W.; Gurney, J.J. In *The properties of diamond*; Field, J.E., Ed.; Academic Press: London, 1979; pp 555-591.

(56) Sobolev, N.V. *Deep-Seated Inclusions in Kimberlites and the Problem of the Composition of the Upper Mantle*; American Geophysical Union: Washington, DC, 1977.

(57) Orlov, J.L. *The mineralogy of Diamond*; Wiley: New York, USA, 1977.

(58) Futergendler, S.I.; Frank-Kamenetsky, V.A. Oriented Inclusions of Olivine, Garnet and Chrome-Spinel in Diamonds. *Zapiski Vsesoyuznogo Mineralogicheskogo Obshestva* **1961**, *90*, 230-236 (in Russian).

(59) Mitchell, R.S.; Giardini, A.A. Oriented Olivine Inclusions in Diamond *Am. Mineral.* **1953**, *38*, 136-138.

(60) Wiggers de Vries, D.F.; Drury, M.R.; de Winter, D.A.M.; Bulanova, G.P.; Pearson, D.G.; Davies, G.R. Three-Dimensional Cathodoluminescence Imaging and Electron Backscatter Diffraction: Tools for Studying the Genetic Nature of Diamond Inclusions. *Contrib. Mineral. Petrol.* **2011**, *161*, 565-579.

(61) Nestola, F.; Nimis, P.; Angel, R.J.; Milani, S.; Bruno, M.; Prencipe, M.; Harris, J.W. *in preparation*.

(62) Spetsius, Z.V.; Belousova, E.A.; Griffin, W.L.; O'Reilly, S.Y.; Pearson, N.J. Archean Sulfide Inclusions in Paleozoic Zircon Megacrysts from the Mir kimberlite, Yakutia: Implications for the Dating of Diamonds. *Earth Planet. Sci. Lett.* **2002**, *199*, 111-126.

Ab initio calculations of the main crystal surfaces of forsterite (Mg₂SiO₄): a preliminary study to understand the nature of geochemical processes at the olivine interface

BRUNO M.,*[1] MASSARO F. R.,[2] PRENCIPE M.,[1] DEMICHELIS R.,[3] DE LA PIERRE M.,[4] NESTOLA F.[2]

[1] Dipartimento di Scienze della Terra, Università degli Studi di Torino, Via Valperga Caluso 35, 10125 Torino, Italy.

[2] Dipartimento di Geoscienze, Università degli Studi di Padova, Via Gradenigo 6, 35131 Padova, Italy.

[3] Nanochemistry Research Institute, Department of Chemistry, Curtin University, PO Box U1987, Perth, WA 6845, Australia.

[4] Dipartimento di Chimica, Università degli Studi di Torino and NIS -Nanostructured Interfaces and Surfaces - Centre of Excellence, Via P. Giuria 7, 10125 Torino, Italy.

Forsterite (Mg₂SiO₄)
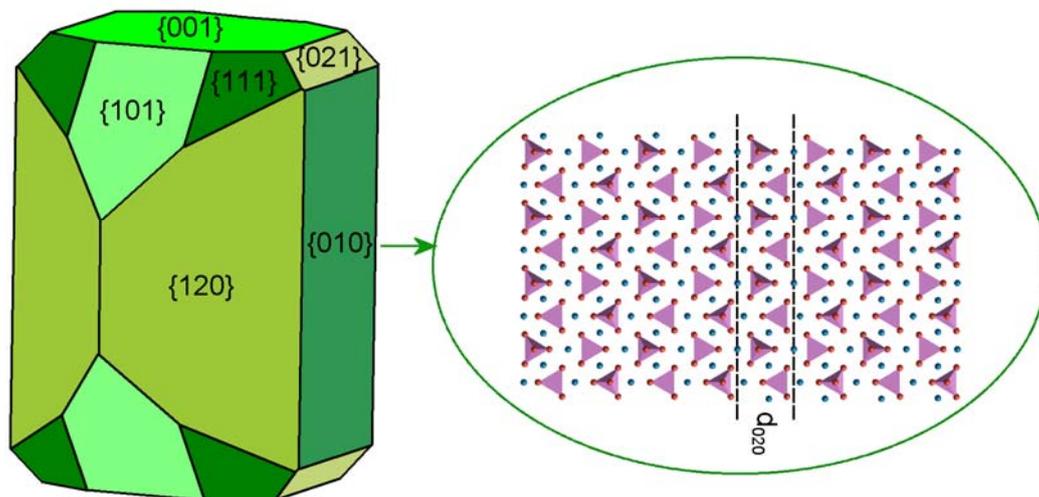
Synopsis

An accurate *ab initio* study of the structure and surface energy at 0 K of the (010), (101), (111), (001), (110), (120) and (021) faces of forsterite (Mg₂SiO₄), by using the hybrid Hartree-Fock/Density Functional B3LYP Hamiltonian and a localized all-electron Gaussian-type basis set, is presented.